Supporting Information

Structural Modifications of $M_5O_4I_{11}$ (M = Nb, Ta) Cluster Networks from Heterogeneous Solid-State Reactions

Fabian Grahlow, Jan Beitlberger, Mario Martin, Eric Juriatti, Heiko Peisert, Marcus Scheele, Markus Ströbele, Carl P. Romao, and Hans-Jürgen Meyer

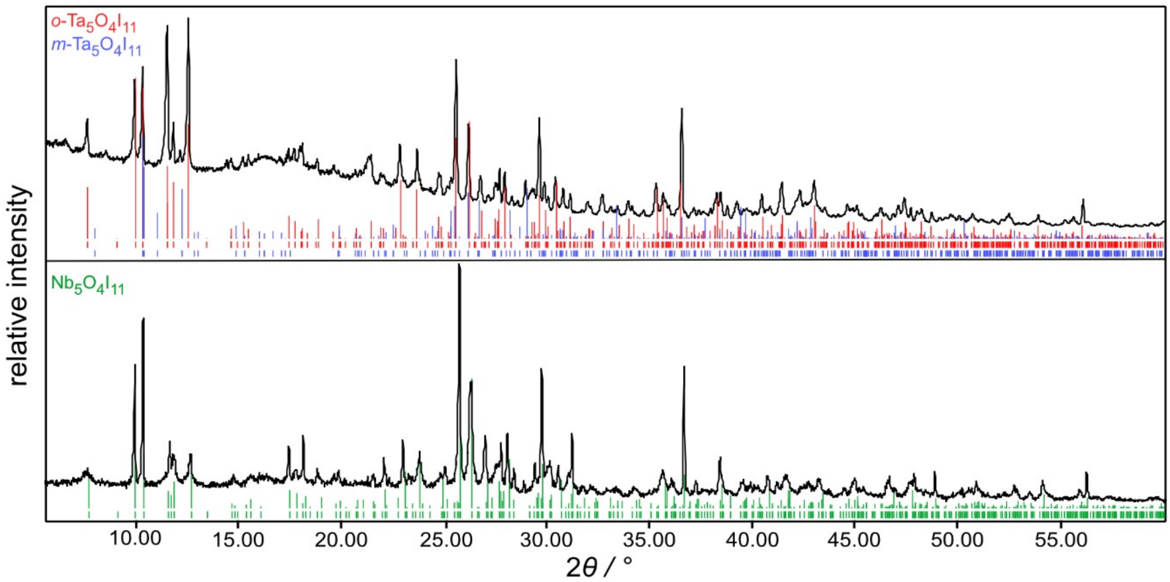

Figure S1. Powder X-ray diffraction patterns of $Ta_5O_4I_{11}$ (orthorhombic and monoclinic) and $Nb_5O_4I_{11}$ with the corresponding Bragg positions, calculated from the single-crystal X-ray diffraction measurements.

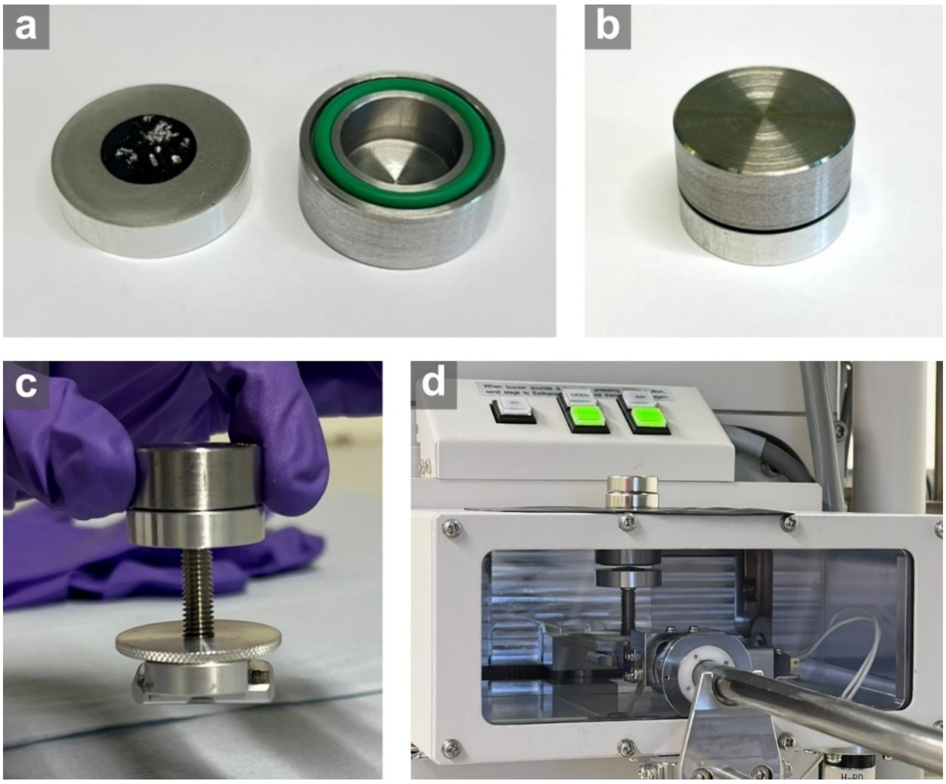

Figure S2. Procedure for inert transfer of samples into the scanning electron microscope. (a) The sample is fixed onto the sample holder using carbon tape. (b) The lid is placed on top of the sample holder, evacuated within the glovebox airlock, and then rapidly flooded with argon to ensure airtight seal. (c) The sealed sample is screwed on the transfer holder and transferred into the SEM airlock, while the reduced-pressure environment maintains the seal. (d) Once the SEM chamber is evacuated, the transfer chamber lid can be lifted using an external magnet.

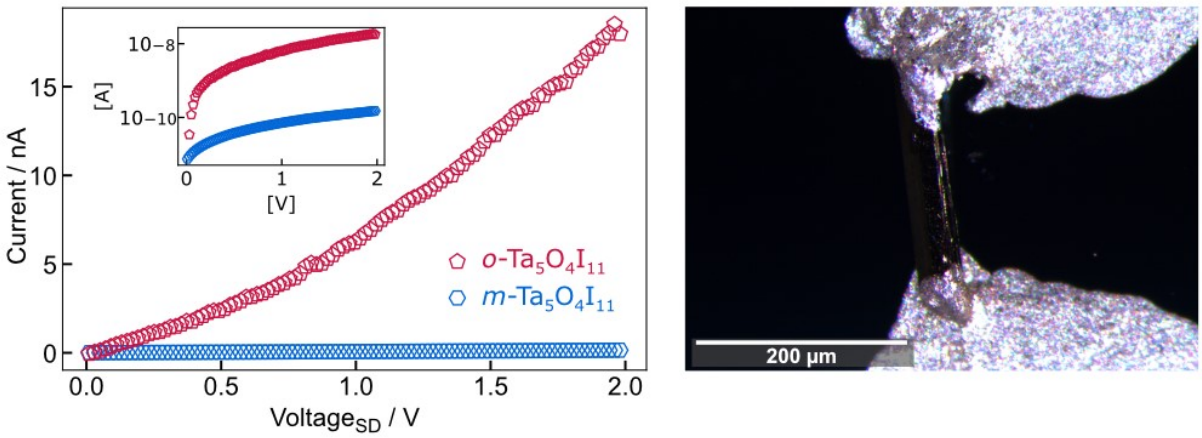

Figure S3. *I*-*U*-sweeps of an *o*-$Ta_5O_4I_{11}$ crystal (red) and a *m*-$Ta_5O_4I_{11}$ crystal (blue) at a temperature of 300 K (left). The inset shows the same data on a logarithmic scale to see the increase of current of *m*-$Ta_5O_4I_{11}$ (left). Single crystals are fixed onto Si/SiO_2 using conductive silver paste (right).

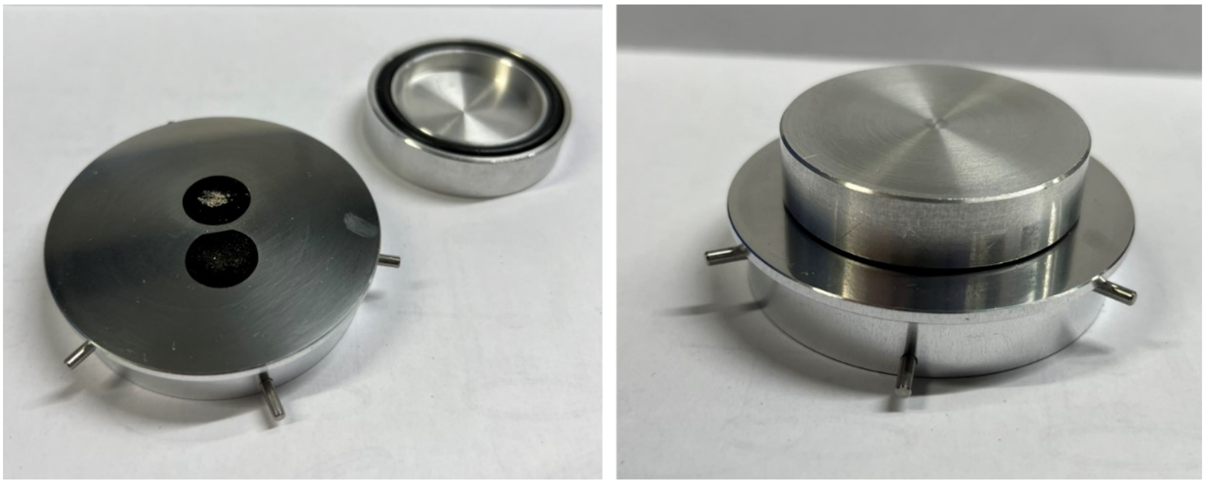

Figure S4. Sample holder and lid for inert transfer for XPS measurements. The sample is fixed onto the sample holder using carbon tape (left). The lid is placed on top of the sample holder, evacuated within the glovebox airlock, and then rapidly flooded with argon to ensure airtight seal (right).

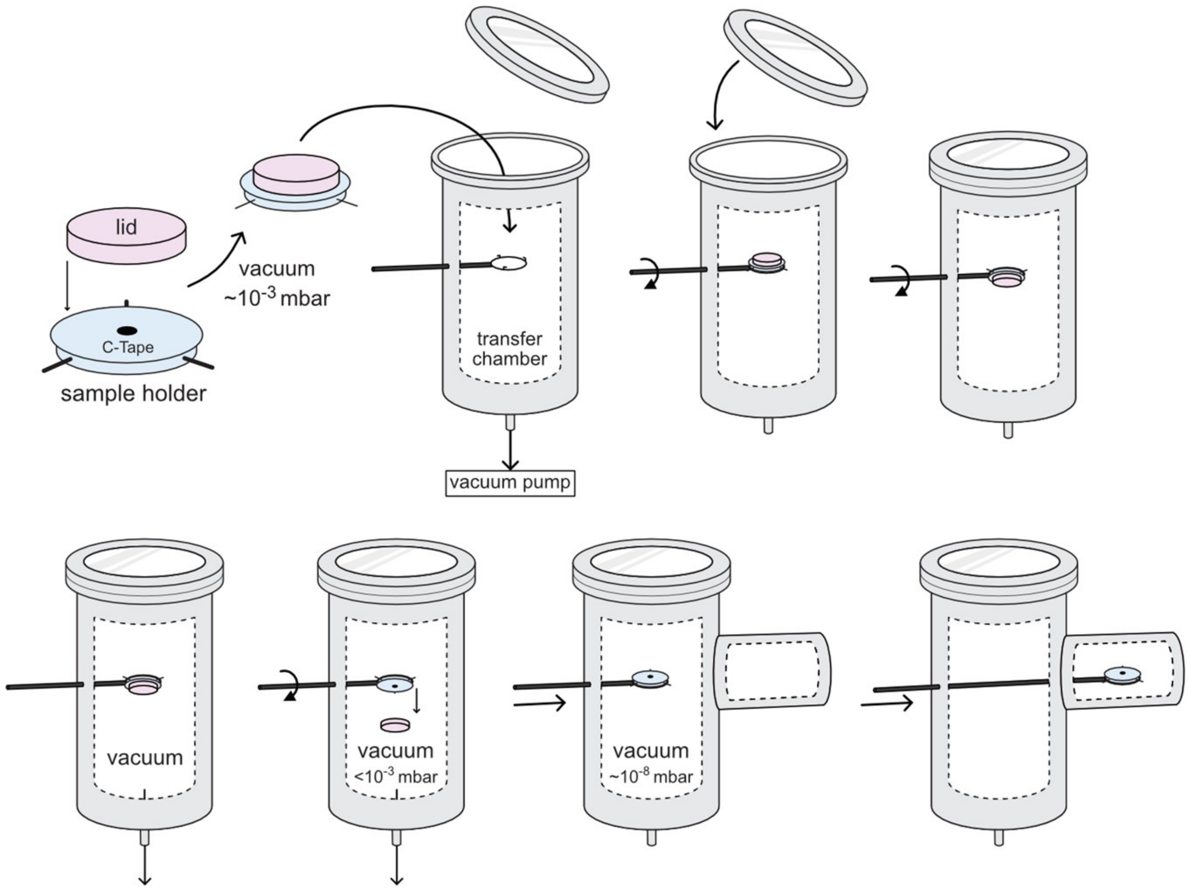

Figure S5. Schematic illustration of the inert transfer procedure for XPS measurements. The sample is mounted on a holder using carbon tape and sealed with a lid under reduces pressure (~10^{-3} mbar) inside a glovebox airlock (compare Figure S4). The sealed holder is then placed into the XPS transfer chamber, which is subsequently closed. From outside the chamber, the sample holder is inverted. As the chamber is evacuated, the internal pressure of the sealed holder becomes higher than the chamber pressure (<10^{-3} mbar), causing the lid to detach and fall to the bottom of the chamber. The pressure is further reduced to ~10^{-8} mbar before the sample is transferred into the XPS measurement chamber.

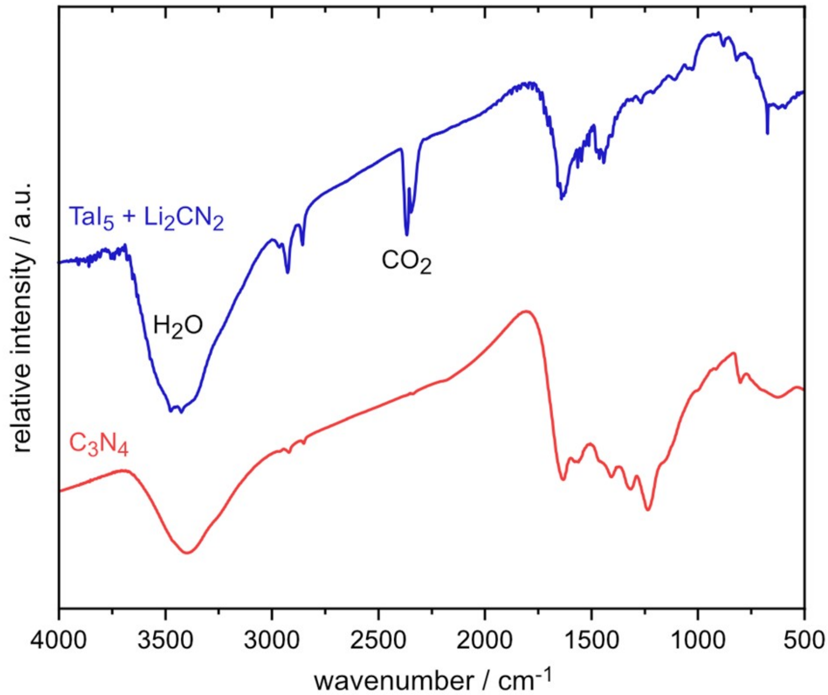

Figure S6. IR spectrum of the product from the reaction of TaI_5 and Li_2CN_2 (blue, top) compared to the IR spectrum of amorphous C_3N_4, synthesized according to literature procedure (red, bottom).[1]

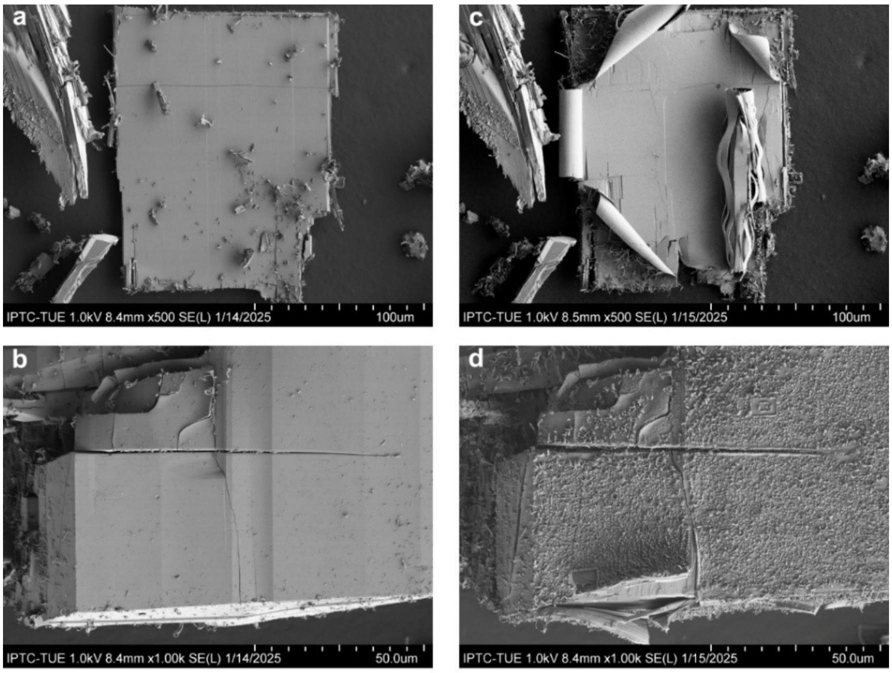

Figure S7. SEM images of two $Ta_5O_4I_{11}$ crystals after inert transfer into the device (a, b), and the corresponding crystals after being exposed to air for five minutes before being re-examined in the SEM (c, d).

[1] H. Zhao, X. Chen, C. Jia, T. Zhou, X. Qu, J. Jian, Y. Xu, T. Zhou, *Materials Science and Engineering: B* **2005**, *122*, 90-93.

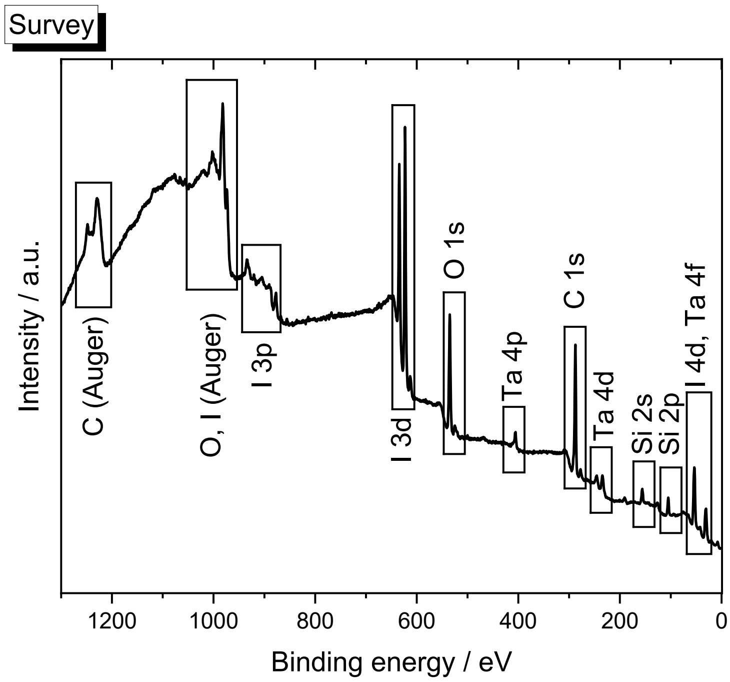

Figure S8. XPS survey spectrum for binding energies of 1300-0 eV showing Ta, I and O signals from the sample and C, Si and O signals from the conductive carbon tape.

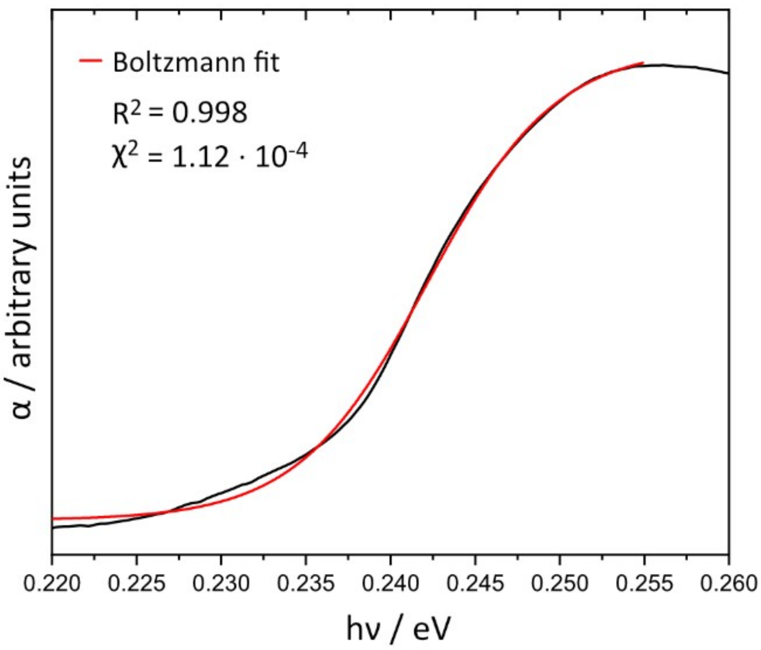

Figure S9. Optical absorption spectrum of *o*-$Ta_5O_4I_{11}$ with the Boltzmann function used to fit *α*.

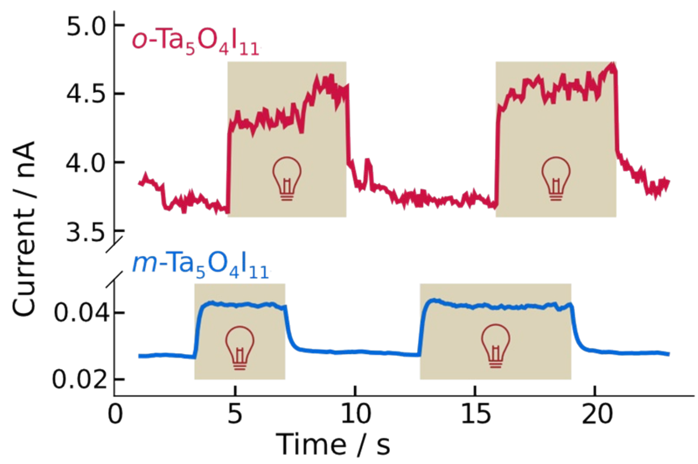

Figure S10. Photoresponse of an *o*-$Ta_5O_4I_{11}$ crystal (top, red) and a *m*-$Ta_5O_4I_{11}$ crystal (bottom, blue) toward a 779 nm laser at 300 K.

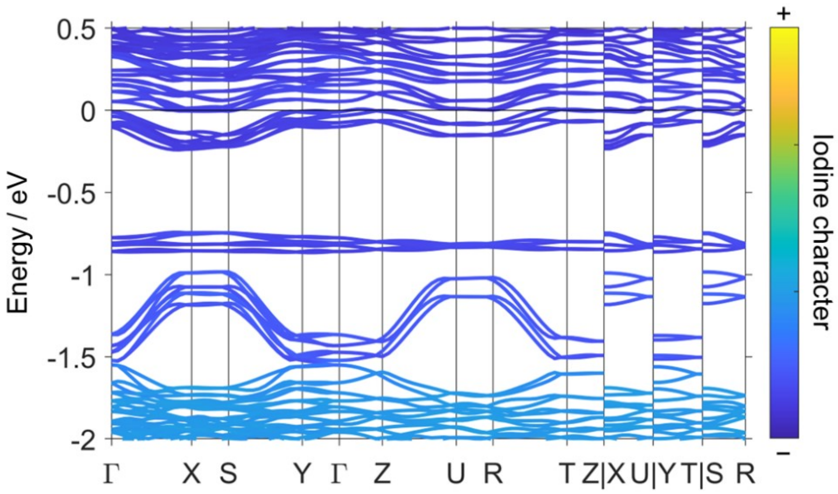

Figure S11. Calculated electronic band structure of *o*-$Ta_5O_4I_{11}$, with bands coloured by their I character. Spin-orbit coupling was included in the calculation. Special points in and paths through reciprocal space were chosen following the literature.[1]

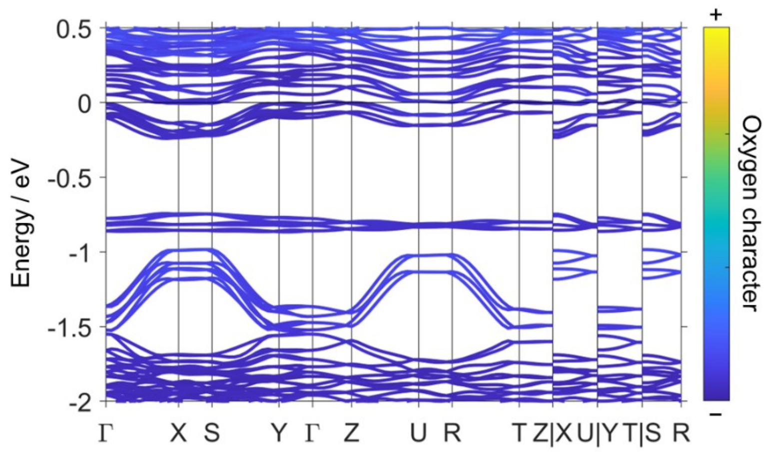

Figure S12. Calculated electronic band structure of *o*-$Ta_5O_4I_{11}$, with bands coloured by their O character. Spin-orbit coupling was included in the calculation. Special points in and paths through reciprocal space were chosen following the literature.[1]

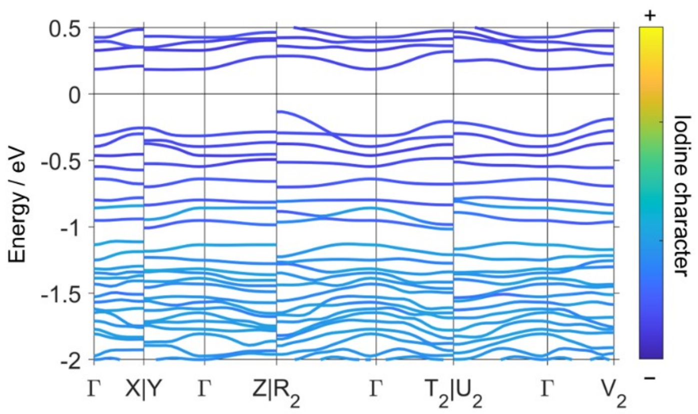

Figure S13. Calculated electronic band structure of *m*-$Ta_5O_4I_{11}$, with bands coloured by their I character. Spin-orbit coupling was included in the calculation. Special points in and paths through reciprocal space were chosen following the literature.[1]

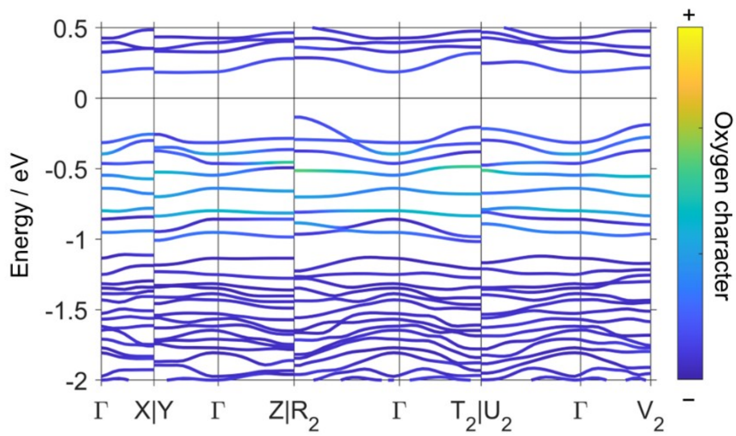

Figure S14. Calculated electronic band structure of *m*-$Ta_5O_4I_{11}$, with bands coloured by their O character. Spin-orbit coupling was included in the calculation. Special points in and paths through reciprocal space were chosen following the literature.[1]

1. Y. Hinuma; G. Pizzi; Y. Kumagai; F. Oba; I. Tanaka. Band structure diagram paths based on crystallography. *Comput. Mater. Sci.* **2017**, *128*, 140-184.

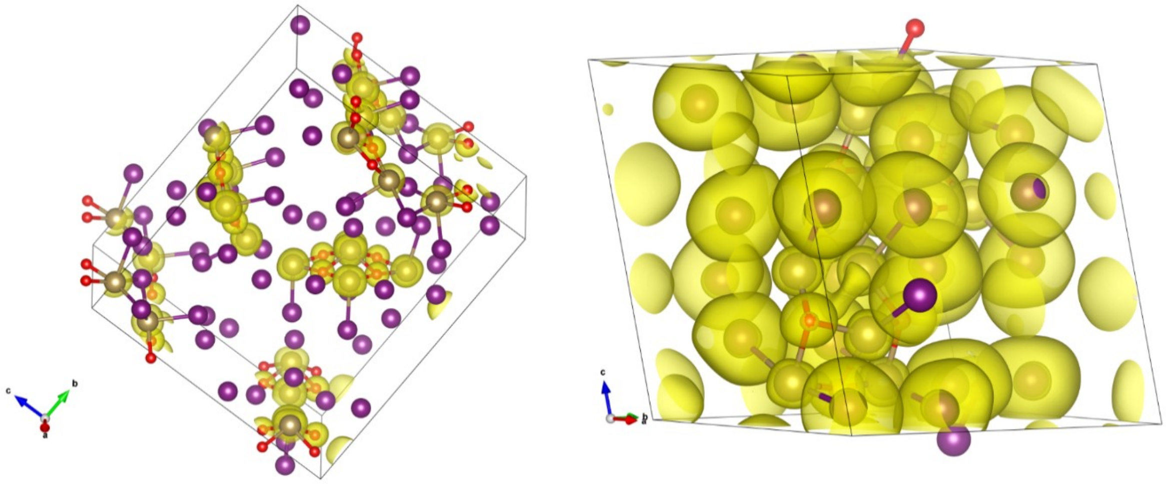

Figure S15. Three-dimensional ELF images of orthorhombic (left) and monoclinic (right) $Ta_5O_4I_{11}$ with isosurfaces at the 0.65 level.

Table S1. Comparison of selected interatomic distances (pm) and bond angles (°) in *m*-$Ta_5O_4I_{11}$ and $Ta_5O_4I_{11}(TaI_5)$.

distance / pm ; ∠ / °	***m*-$Ta_5O_4I_{11}$**	**distance / pm ; ∠ / °**	**$Ta_5O_4I_{11}(TaI_5)$**
intra cluster		**intra cluster**	
Ta(1) – Ta(2)	286.34(3)	Ta(1) – Ta(5)	286.91(4)
Ta(1) – Ta(3)	286.97(3)	Ta(1) – Ta(2)	287.66(4)
		Ta(1) – Ta(3)	287.17(4)
		Ta(1) – Ta(4)	287.57(4)
∠ Ta(2) – Ta(1) – Ta(3)	132.21(1)	∠ Ta(3) – Ta(1) – Ta(5)	131.33(1)
		∠ Ta(2) – Ta(1) – Ta(4)	130.57(1)
inter cluster		**inter cluster**	
Ta(2) – Ta(3)	443.17(4)	Ta(2) – Ta(3)	439.06(5)
Ta(4) – Ta(5)	434.12(3)	Ta(4) – Ta(5)	433.71(7)

Table S2. XPS-fit parameters for the Ta 4f spectrum depicted in Figure 11.

	Position (eV)	Gaussian width (eV)	Lorentzian width (eV)	rel. area (%)
Ta^{4+} $4f_{7/2}$	26.35	1.65	0.30	46.1
Ta^{4+} $4f_{5/2}$	28.23	1.65	0.30	34.5
Ta^{3+} $4f_{7/2}$	24.23	2.50	0.50	11.1
Ta^{3+} $4f_{5/2}$	26.10	2.50	0.50	8.3

Table S3. Crystallographic data of $M_5O_4I_{11}$ (M = Nb, Ta) cluster compounds.

	$Nb_5O_4I_{11}$	*o*-$Ta_5O_4I_{11}$	*m*-$Ta_5O_4I_{11}$	$Ta_5O_4I_{11}(TaI_5)$
CCDC Identification code	2400835	2380271	2424946	2351105
Formula weight	1924.45	2364.65	2364.65	3180.10
Radiation type	Cu K_α	Mo K_α	Mo K_α	Mo K_α
Wavelength / pm	154.184	71.073	71.073	71.073
Crystal system	orthorhombic	orthorhombic	monoclinic	orthorhombic
Space group	$Pmc2_1$	$Pmc2_1$	$P2_1/m$	$Pbca$
Unit cell dimensions / Å	a = 9.7963(2) b = 17.8082(3) c = 15.2052(2)	a = 9.8198(1) b = 17.8539(1) c = 15.3672(1)	a = 8.9594(1) b = 13.6077(1) c = 15.3672(1) β = 107.500(2)	a = 17.7586(3) b = 13.4107(4) c = 30.4660(6)
Volume / $Å^3$	2652.61(8)	2694.20(4)	1351.20(3)	7255.6(3)
Z	4	4	2	8
Density (calculated) / g cm^{-3}	4.819	5.830	5.812	5.822
Absorption coefficient / mm^{-1}	117.683	32.835	32.735	31.645
Crystal size / mm^3	0.09×0.05×0.01	0.36×0.04×0.04	0.18×0.09×0.03	0.14×0.02×0.01
Theta range for data collection	3.823° to 68.216°	2.074° to 30.507°	2.370° to 25.344°	2.017° to 25.350°
Reflections collected	10180	128478	39410	53383
Independent reflections	4407	8650	2583	6642
R_{int}	0.0339	0.0403	0.0303	0.0507
restraints / parameters	1 / 208	1 / 206	0 / 98	0 / 245
Goodness-of-fit on F^2	1.025	1.102	1.479	1.015
Final R indices [$I > 2\sigma(I)$]	R_1 = 0.0485 wR_2 = 0.1254	R_1 = 0.0215 wR_2 = 0.0560	R_1 = 0.0154 wR_2 = 0.0342	R_1 = 0.0226 wR_2 = 0.0443
R indices (all data)	R_1 = 0.0515 wR_2 = 0.1270	R_1 = 0.0218 wR_2 = 0.0561	R_1 = 0.0154 wR_2 = 0.0343	R_1 = 0.0305 wR_2 = 0.0464
Largest diff. peak and hole	1.205 and -0.493 e·$Å^{-3}$	1.509 and -1.157 e·$Å^{-3}$	0.759 and -0.731 e·$Å^{-3}$	1.946 and -1.789 e·$Å^{-3}$